

LANL Report LA-UR-00-3597, Los Alamos (2000)

Proc. SATIF5, July 18-21, 2000, Paris, France

**STUDY OF RESIDUAL PRODUCT NUCLIDE YIELDS IN 1.0 GEV
PROTON-IRRADIATED ^{208}Pb AND 2.6 GEV PROTON-IRRADIATED ^{nat}W
THIN TARGETS**

**Yury E. Titarenko, Oleg V. Shvedov, Vyacheslav F. Batyaev, Valery M. Zhivun,
Evgeny I. Karpikhin, Ruslan D. Mulambetov, Dmitry V. Fischenko,
Svetlana V. Kvasova**

Institute for Theoretical and Experimental Physics, B. Cheremushkinskaya 25, 117259
Moscow, Russia

Stepan G. Mashnik, Richard E. Prael, Arnold J. Sierk
Los Alamos National Laboratory, Los Alamos, NM 87545, USA

Hideshi Yasuda
Japan Atomic Energy Research Institute, Tokai, Ibaraki, 319-1195, Japan

Abstract

113 residual product nuclide yields in a 1.0 GeV proton-irradiated thin monoisotopic ^{208}Pb sample and 107 residual product nuclide yields in a 2.6 GeV proton-irradiated ^{nat}W sample have been measured and simulated by 8 different codes. The irradiations were made using proton beams extracted from the ITEP synchrotron. The nuclide yields were γ -spectrometered directly using a high-resolution Ge-detector. The γ -spectra were processed by the GENIE-2000 code. The ITEP-developed SIGMA code was used together with the PCNUDAT nuclear decay database to identify the γ -lines and to determine the cross-sections. The $^{27}\text{Al}(p,x)^{22}\text{Na}$ reaction was used to monitor the proton flux. The measured yields are compared with calculation the LAHET (with ISABEL and Bertini options), CEM95, CEM2k, CASCADE, CASCADE/INPE, INUCL, and YIELDX codes. Estimates of the mean deviation factor are used to demonstrate the predictive power of the codes. The results obtained may be of interest in studying the parameters of the Pb and W target modules of the hybrid Accelerator-Driven System (ADS) facilities.

Introduction

At present, the Pb-Bi eutectic and W are regarded as the most promising target materials for ADS facilities [1]-[3]. As a result, the high-energy irradiation mode of using the materials necessitates additional studies of the nuclear-physics characteristics of Pb, Bi, and W, particularly the yields of residual product nuclei under proton irradiation in a broad range of energies from a few MeV to 2-3 GeV. Results of such studies are extremely important when designing even demonstration versions of the ADS facilities.

Undoubtedly, computational methods will play an important role when forming a set of nuclear constants for ADS facilities. Therefore, verification of the most extensively used simulation codes has proved to be of a high priority.

Basic definitions and computational relations

The formalism of representing the reaction product yields (cross sections) in high-energy proton-irradiated thin targets is described in sufficient detail in [4]. In terms of the formalism, the variations in the concentration of any two chain nuclides produced in an irradiated target ($N_1 \xrightarrow{\lambda_1} N_2 \xrightarrow{\lambda_2}$) may be presented to be a set of differential equations that describe the production and decays of the nuclides. By introducing a formal representation of the time functions, F_i , of the form $F_i = (1 - e^{-\lambda_i \tau}) \frac{1 - e^{-\lambda_i K T}}{1 - e^{-\lambda_i T}}$, ($i=1, 2$, and Na or another monitor product; τ is the duration of a single proton pulse; T is the pulse repetition period; K is the number of pulses within the irradiation period), which characterize the nuclide decays within the irradiation time, and by expressing (similar to the relative measurements) the proton fluence size via the monitor reaction cross section, σ_{st} , we can present the cumulative and independent yields as:

$$\sigma_1^{cum} = \frac{A_0}{\eta_1 \varepsilon_1 F_1 N_{Na}} \frac{N_{Al} F_{Na}}{N_T \lambda_{Na}} \sigma_{st} \quad (1)$$

$$\sigma_1^{cum} = \frac{A_1}{\nu_1 \eta_2 \varepsilon_2 F_1 N_{Na}} \frac{N_{Al} \lambda_2 - \lambda_1 F_{Na}}{N_T \lambda_2 \lambda_{Na}} \sigma_{st} \quad (2)$$

$$\sigma_2^{ind} = \left(\frac{A_2}{F_2} + \frac{A_1 \lambda_1}{F_1 \lambda_2} \right) \frac{1}{\eta_2 \varepsilon_2 N_{Na}} \frac{N_{Al} F_{Na}}{N_T \lambda_{Na}} \sigma_{st} \quad (3)$$

$$\sigma_2^{cum} = \sigma_2^{ind} + \nu_1 \sigma_1^{cum} = \left(\frac{A_1}{F_1} + \frac{A_2}{F_2} \right) \frac{1}{\eta_2 \varepsilon_2 N_{Na}} \frac{N_{Al} F_{Na}}{N_T \lambda_{Na}} \sigma_{st} , \quad (4)$$

where σ_1^{cum} is the cumulative cross section of the first nuclide; σ_2^{ind} and σ_2^{cum} are the independent and cumulative cross sections of the second nuclide; N_{Al} and N_T are the numbers of nuclei in the monitor (standard) and in experimental sample, respectively; η_1 and η_2 are the γ -line yields; ε_1 and ε_2 are the spectrometer efficiencies at energies E_{γ_1} and E_{γ_2} ; ν_1 is the branching ratio of the first nuclide; λ_1 , λ_2 , and λ_{Na} are, respectively, the decay constants of the first and second nuclides and of the monitor product (^{22}Na and/or ^{24}Na).

The factors A_0 , A_1 , and A_2 are calculated through fitting the measured counting rates in the total absorption peaks, which correspond to energies E_{γ_1} (the first nuclide) and E_{γ_2} (the

second nuclide), by exponential functions. It should be noted that formulas (1)–(4) were derived on assumption that the γ -intensities of the two nuclides produced under irradiation are recorded up to the desired accuracy within an interval of time from the irradiation end to the moment of the ultimate detectable intensity. If, for some reasons, the factor A_1 cannot be found, then the factor A_2 will be used together with expression (14) from [4] to determine the quantity σ_2^{cum*} , which we called the supra cumulative yield:

$$\begin{aligned}\sigma_2^{cum*} &= \sigma_2 + \frac{\lambda_2}{\lambda_1 - \lambda_2} \nu_1 \sigma_1^{cum} = \\ &= \frac{A_2}{\eta_2 \varepsilon_2 F_2 N_{Na}} \frac{N_{Al}}{N_T} \frac{F_{Na}}{\lambda_{Na}} \sigma_{st}\end{aligned}\quad (5)$$

The resultant value of σ_2^{cum*} may prove to be very different from σ_2^{cum} . Nevertheless, the supra cumulative yield can be either used directly to verify the codes, or determined further up to σ_2^{cum} if the needed data are obtained elsewhere (for example, from inverse-kinematics experiments).

Experimental techniques

A 10.5 mm diameter, 139.4 mg/cm² monoisotopic ²⁰⁸Pb metal foil sample (97.2% ²⁰⁸Pb, 1.93% ²⁰⁷Pb, 0.87% ²⁰⁶Pb, <0.01% ²⁰⁴Pb, < 0.00105% of chemical impurities) and a 38.1 mg/cm² ^{nat}W metal foil sample (99.95% W, <0.05% of chemical impurities), both of 10.5-cm diameter, were proton-irradiated. 139.6 mg/cm² and 139.1 mg/cm² Al foils of the same diameter were used as monitors. Chemical impurities of the monitor did not exceed 0.001%.

The samples were irradiated by the external proton beam from the ITEP U-10 synchrotron [4]. The average flux densities during irradiation of Pb and W samples were of 1.4×10^{10} p/cm² and 2.8×10^{10} p/cm², respectively.

Our measurements were supported by extra researches aimed at reducing the systematic errors in the experimental results. Theses researches included:

- experiments to specify the neutron component in the extracted proton beams,
- experiments to specify the ²⁷Al(p,x)²⁴Na monitor reaction cross section,
- studies to specify the dependence of the γ -spectrometer detection efficiency on the position geometry of irradiated sample,
- studies to optimize the γ -spectrum simulation codes.

Figs. 1 and 2 show the results of measuring the neutron component in the extracted proton beams, i.e., the neutron-to-proton flux density ratio, Φ_n/Φ_p . Fig. 3 presents the monitor reaction cross sections measured here and in other works¹. The height-energy dependence of the detection efficiency is displayed in Fig. 4.

¹ MI85 – Nucl. Phys. A **441** (1985) 617; MI86 – NIM B **16** (1986) 61; MI89 – Analyst **114** (1989) 287; Mi90 – NEANDC(E)-312-U(1990) 46; MI93 – INDC(GER)-037/LN(1993) 49; MI95 – NIM B **103** (1995) 183; MI96 – NIM B **114** (1996) 91; MI97 – NIM B **129** (1997) 153.

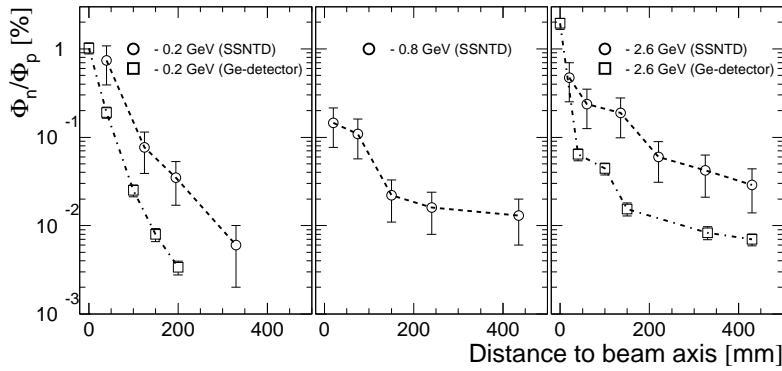


Figure 1: The neutron backgrounds around the extracted proton beams that irradiate thin experimental samples.

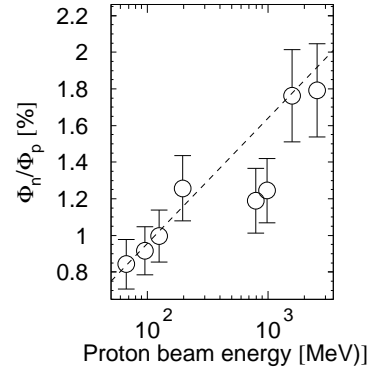


Figure 2: Neutron component in the extracted proton beams of different energies.

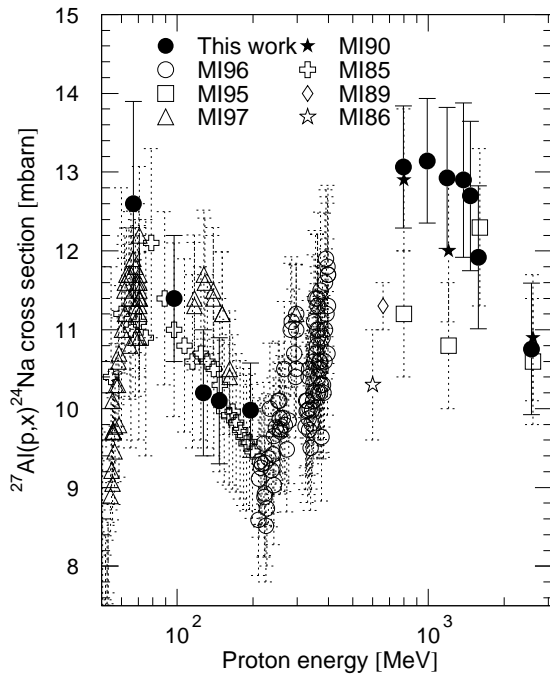


Figure 3: The $^{27}\text{Al}(p,x)^{24}\text{Na}$ monitor reaction cross sections measured in this and other works.

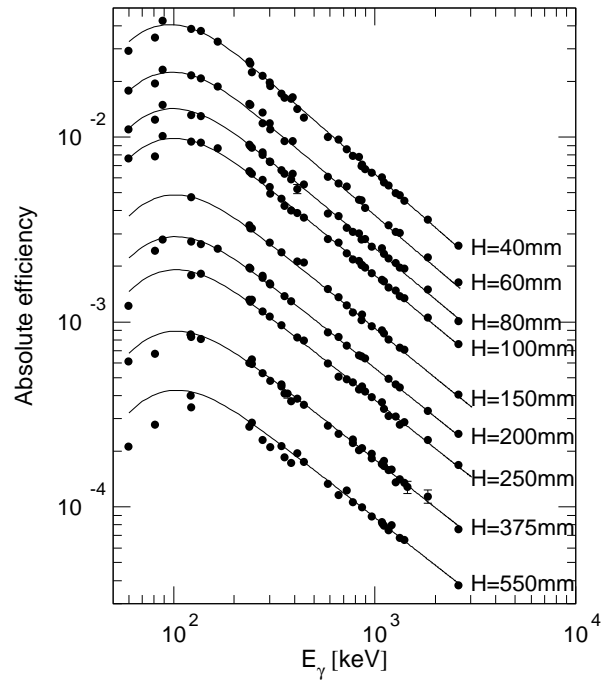


Figure 4: The experimental and calculated detection efficiency of the spectrometer.

The discrepancies between the two sets of high-energy data in Fig. 3 have yet to be studied. The analytical expression of the spectrometer detection efficiency as a function of energy and sample position height is

$$\varepsilon(E, H) = \varepsilon_{base}(E) \cdot \left[\frac{(q_1 + q_2 \cdot \ln E + H_{base})}{(q_1 + q_2 \cdot \ln E + H)} \right]^2, \quad (6)$$

where q_1 and q_2 are parameters defined by fitting the experimental results. An analysis of the γ -spectrum processing codes has shown that the GENIE-2000 code is superior to the others because of its interactive mode of fitting the peaks, which permits correction of the automated computer-aided processing; therefore, we chose it for our work.

Experimental results and measurement errors

Tables 1 and 2 present the results of measuring the reaction product yields in the 1 GeV proton-irradiated ^{208}Pb and 2.6 GeV proton-irradiated ^{nat}W samples. 113 yields from ^{208}Pb have been obtained, of which, 6 independent yields (i), 17 independent yields of metastable states (m), 15 independent yields of metastable and ground states ($\Sigma m_j + g$), 64 cumulative yields (c), and 11 supra cumulative yields, when the addend may exceed the determination error (c^*). 107 yields from ^{nat}W are presented, of which, 6 independent yields (i), 9 metastable state yields (m), 5 yields of metastable and ground states ($\Sigma m_j + g$), 86 cumulative yields (c), and 1 supra cumulative yield (c^*).

From Tables 1 and 2 one can see that the experimental errors are ranging within $\sim(6-35)\%$. The main contribution to the total error is from uncertainties in the nuclear data, namely, in the absolute quantum yields and cross sections of the monitor reactions.

Comparison with experimental data obtained elsewhere

Table 3 and Fig. 9 compare some of the present results with experimental data of other laboratories published in [6].

Table 1: Experimental product nuclide yields in 1 GeV proton-irradiated ^{208}Pb

Product	$T_{1/2}$	Type	Yield (mb)
^{206}Bi	6.243d	i	4.60 ± 0.29
^{205}Bi	15.31d	i	6.20 ± 0.40
^{204}Bi	11.22h	i(m1+m2+g)	5.29 ± 0.80
^{203}Bi	11.76h	i(m+g)	4.84 ± 0.59
^{204m}Pb	67.2m	i(m)	11.0 ± 1.0
^{203}Pb	51.873h	c	31.5 ± 2.1
^{201}Pb	9.33h	c^*	26.9 ± 2.4
^{200}Pb	21.5h	c	18.2 ± 1.2
^{198}Pb	2.4h	c	8.9 ± 2.1
^{197m}Pb	43.0m	c^*	17.9 ± 4.0
^{202}Tl	12.23d	c	18.9 ± 1.2

Continuation of Table 1

Product	$T_{1/2}$	Type	Yield (mb)
^{201}Tl	72.912h	c	43.7 ± 2.9
^{200}Tl	26.1h	c	40.6 ± 2.6
^{200}Tl	26.1h	i(m+g)	22.7 ± 1.5
^{199}Tl	7.42h	c	38.5 ± 5.2
$^{198m1}\text{Tl}$	1.87h	i(m1+m2)	17.6 ± 3.6
^{198}Tl	5.30h	c	35.9 ± 5.0
^{196m}Tl	84.6m	i(m)	34.8 ± 4.4
^{203}Hg	46.612d	c	4.03 ± 0.27
^{197m}Hg	23.8h	i(m)	10.7 ± 0.7
^{195m}Hg	41.6h	i(m)	13.6 ± 2.0
^{193m}Hg	11.8h	i(m)	18.9 ± 2.5
^{192}Hg	4.85h	c	35.2 ± 2.8
^{198m}Au	54.48h	i(m)	1.01 ± 0.14
^{198}Au	64.684h	i(m+g)	2.11 ± 0.22
^{198}Au	64.684h	i	1.09 ± 0.30
^{196}Au	6.183d	i(m1+m2+g)	4.13 ± 0.35
^{195}Au	186.098d	c	48.7 ± 5.5
^{194}Au	38.020h	i(m1+m2+g)	7.06 ± 0.75
^{192}Au	4.94h	c	46.9 ± 6.6
^{192}Au	4.94h	i(m1+m2+g)	11.6 ± 1.7
^{191}Pt	69.6h	c	40.1 ± 4.4
^{189}Pt	10.87h	c	46.8 ± 4.8
^{188}Pt	10.2d	c	40.5 ± 2.9
^{190}Ir	11.78d	c	0.69 ± 0.06
^{188}Ir	41.5h	c	43.2 ± 3.2
^{188}Ir	41.5h	i(m+g)	2.93 ± 0.69
^{186}Ir	16.64h	c*	20.8 ± 1.9
^{185}Ir	14.4h	c*	34.8 ± 2.3
^{184}Ir	3.09h	c*	39.5 ± 3.0
^{185}Os	93.6d	c	41.8 ± 2.8
^{183m}Os	9.9h	i(m)	23.2 ± 1.5
^{182}Os	22.1h	c	42.0 ± 2.8
^{183}Re	70.0d	c	41.7 ± 2.9
^{182}Re	12.7h	c	45.2 ± 3.7
^{181}Re	19.9h	c	43.1 ± 5.9
^{179}Re	19.7m	c*	47.8 ± 4.2
^{177}W	2.25h	c	30.1 ± 3.5
^{176}W	2.30h	c	30.8 ± 4.3
^{176}Ta	8.09h	c	34.5 ± 3.6
^{173}Ta	3.14h	c	31.0 ± 3.9
^{172}Ta	36.8m	c*	17.3 ± 2.3
^{175}Hf	70.0d	c	31.3 ± 2.3
^{173}Hf	23.6h	c	28.4 ± 2.6
^{172}Hf	683.017d	c	24.1 ± 1.6
^{171}Hf	12.1h	c	18.2 ± 2.8
^{170}Hf	16.01h	c	22.1 ± 6.8
^{172}Lu	6.7d	c	23.9 ± 1.7
^{172}Lu	6.7d	i(m+g)	0.19 ± 0.05
^{171}Lu	8.24d	c	26.1 ± 1.8
^{170}Lu	48.288h	c	21.7 ± 2.9

Continuation of Table 1

Product	$T_{1/2}$	Type	Yield (mb)
¹⁶⁹ Lu	34.06h	c	18.6± 1.2
¹⁶⁹ Yb	32.026d	c	20.9± 1.5
¹⁶⁶ Yb	56.7h	c	16.1± 1.1
¹⁶⁷ Tm	9.25d	c	19.4± 4.0
¹⁶⁵ Tm	30.06h	c	14.4± 1.4
¹⁶⁰ Er	28.58h	c	8.8± 0.6
¹⁵⁷ Dy	8.14h	c	5.73± 0.45
¹⁵⁵ Dy	9.90h	c*	3.66± 0.27
¹⁵⁵ Tb	5.32d	c	4.16± 0.39
¹⁵³ Tb	56.16h	c*	2.52± 0.25
¹⁵² Tb	17.50h	c*	2.10± 0.17
¹⁵³ Gd	241.6d	c	2.60± 0.23
¹⁴⁹ Gd	9.28d	c	2.24± 0.18
¹⁴⁶ Gd	48.27d	c	1.26± 0.09
¹⁴⁷ Eu	24.0d	c	0.98± 0.31
¹⁴⁶ Eu	4.59d	c	1.63± 0.11
¹⁴⁶ Eu	4.59d	i	0.37± 0.05
¹⁴³ Pm	265.0d	c	1.02± 0.13
¹³⁹ Ce	137.64d	c	0.83± 0.06
^{121m} Te	154.0d	i(m)	0.44± 0.04
¹²¹ Te	16.78d	c	1.11± 0.11
^{119m} Te	4.7d	i(m)	0.40± 0.04
^{120m} Sb	5.76d	i(m)	0.54± 0.05
^{114m} In	49.51d	i(m1+m2)	0.95± 0.19
^{110m} Ag	249.79d	i(m)	1.12± 0.09
^{106m} Ag	8.28d	i(m)	0.89± 0.08
¹⁰⁵ Ag	41.29d	c	0.65± 0.12
¹⁰⁵ Rh	35.36h	c	4.63± 0.54
^{101m} Rh	4.34d	i(m)	1.29± 0.16
¹⁰³ Ru	39.26d	c	3.84± 0.26
⁹⁶ Tc	4.28d	i(m+g)	1.20± 0.09
⁹⁵ Tc	20.0h	c	1.38± 0.13
⁹⁶ Nb	23.35h	i	2.31± 0.19
⁹⁵ Nb	34.975d	c	5.41± 0.34
⁹⁵ Nb	34.975d	i(m+g)	3.03± 0.20
⁹⁵ Zr	64.02d	c	2.34± 0.15
⁸⁹ Zr	78.41h	c	2.30± 0.16
⁸⁸ Zr	83.4d	c	0.76± 0.08
^{90m} Y	3.19h	i(m)	4.82± 0.39
⁸⁸ Y	106.65d	c	4.03± 0.27
⁸⁸ Y	106.650d	i(m+g)	3.41± 0.25
⁸⁷ Y	79.8h	c*	2.94± 0.23
⁸⁵ Sr	64.84d	c	2.76 ± 0.22
⁸⁶ Rb	18.631d	i(m+g)	5.48 ± 0.66
⁸³ Rb	86.2d	c	3.46 ± 0.28
^{82m} Rb	6.472h	i(m)	2.73 ± 0.30
⁸² Br	35.3h	i(m+g)	2.17 ± 0.14
⁷⁵ Se	119.77d	c	1.34 ± 0.09
⁷⁴ As	17.77d	i	1.86 ± 0.18
⁵⁹ Fe	44.503d	c	0.91 ± 0.08
⁶⁵ Zn	244.26d	c	0.79 ± 0.19
⁴⁶ Sc	83.81d	i(m+g)	0.35 ± 0.06

Table 2: Experimental product nuclide yields in 2.6 GeV proton-irradiated ^{nat}W

Product	$T_{1/2}$	Type	Yield (mb)
^{177}W	2.25h	c	13.9 ± 1.9
^{176}W	2.30h	c	9.9 ± 2.9
^{184}Ta	8.7h	c	4.44 ± 0.43
^{183}Ta	5.1d	c	10.5 ± 1.0
^{182}Ta	114.43d	c	12.9 ± 1.3
^{178m}Ta	2.36h	i(m)	8.1 ± 1.3
^{176}Ta	8.09h	c	29.3 ± 3.3
^{175}Ta	10.5h	c	26.0 ± 2.8
^{174}Ta	63m	c	25.8 ± 2.8
^{181}Hf	42.39	c	1.26 ± 0.12
^{173}Hf	23.6h	c	29.9 ± 2.5
^{171}Hf	12.1h	c	19.6 ± 2.4
^{170}Hf	16.01h	c	19.6 ± 4.0
^{172}Lu	6.7d	i(m+g)	4.32 ± 0.56
^{171}Lu	8.24d	c	30.1 ± 2.46
^{171}Lu	8.24d	i(m+g)	10.8 ± 2.0
^{170}Lu	48.288h	c	24.8 ± 2.2
^{169}Lu	34.06h	c	22.2 ± 1.8
^{167}Lu	51.5m	c	23.4 ± 2.4
^{167}Yb	17.5m	c	24.9 ± 2.8
^{166}Yb	56.7h	c	24.6 ± 2.1
^{166}Tm	7.7h	c	27.2 ± 2.3
^{166}Tm	7.7h	i	2.36 ± 0.46
^{165}Tm	30.06h	c	27.1 ± 2.4
^{163}Tm	1.81h	c	26.3 ± 3.3
^{161}Tm	33m	c	21.0 ± 2.5
^{161}Er	3.21h	c	24.3 ± 2.5
^{160}Er	28.58h	c	23.9 ± 2.2
^{157}Er	25m	c	26.4 ± 5.9
^{156}Er	19.5m	c	15.9 ± 2.4
$^{160m1}\text{Ho}$	5.02h	i(m1+m2)	24.9 ± 2.3
^{157}Ho	12.6m	c	26.1 ± 6.8
^{156}Ho	56m	c	19.6 ± 1.8
^{157}Dy	8.14h	c	24.2 ± 2.2
^{155}Dy	9.90h	c	22.1 ± 1.9
^{153}Dy	6.4h	c	14.0 ± 1.9
^{152}Dy	2.38h	c	15.6 ± 1.3
^{155}Tb	5.32d	c	22.7 ± 1.9
^{153}Tb	56.16h	c	18.9 ± 1.7
^{152}Tb	17.50h	c	16.2 ± 1.3
^{151}Tb	17.609h	c	16.7 ± 1.4
^{149}Tb	4.118h	c	6.85 ± 0.62
^{147}Tb	1.70h	c	2.15 ± 0.34
^{151}Gd	124.0d	c	19.0 ± 2.2
^{149}Gd	9.28d	c	20.4 ± 1.7
^{147}Gd	38.1h	c	18.6 ± 1.6
^{146}Gd	48.27d	c	19.4 ± 1.6
^{145}Gd	23.0m	c	12.9 ± 1.4
^{149}Eu	93.1d	c	26.7 ± 3.4

Continuation of Table 2

Product	T _{1/2}	Type	Yield (mb)
¹⁴⁷ Eu	24.0d	c	22.4 ± 2.0
¹⁴⁶ Eu	4.59d	c	23.0 ± 1.9
¹⁴⁶ Eu	4.59d	i	3.62 ± 0.31
¹⁴⁵ Eu	5.93d	c	17.8 ± 1.6
¹³⁹ Nd	5.5h	c	2.87 ± 0.43
¹³⁹ Ce	137.64d	c	19.8 ± 1.6
¹³⁵ Ce	17.7h	c	17.8 ± 1.5
¹³² Ce	3.51h	c	16.3 ± 2.7
¹³² La	4.8h	c	14.5 ± 1.6
¹³¹ Ba	11.50d	c	16.2 ± 1.3
¹²⁶ Ba	100m	c	7.9 ± 1.1
¹²⁹ Cs	32.06h	c	18.7 ± 1.6
¹²⁷ Xe	36.4d	c	15.4 ± 1.3
¹²⁵ Xe	16.9h	c	14.2 ± 1.2
¹²³ Xe	2.08h	c	15.6 ± 1.3
¹²² Xe	20.1h	c	11.7 ± 1.0
¹²¹ Te	16.78d	c	10.7 ± 1.1
¹¹⁹ Te	16.03h	c	9.17 ± 0.74
^{119m} Te	4.7d	i(m)	1.97 ± 0.17
¹¹⁷ Te	62m	c	8.81 ± 0.77
^{118m} Sb	5.0h	i(m)	1.08 ± 0.22
¹¹⁵ Sb	32.1m	*	9.85 ± 0.88
¹¹³ Sn	115.09d		7.55 ± 0.67
¹¹¹ In	2.8049d		7.44 ± 0.74
^{110m} In	4.9h	i(m)	3.29 ± 0.29
¹⁰⁹ In	4.2h	c	5.12 ± 0.43
^{106m} Ag	8.28d	i(m)	1.70 ± 0.16
¹⁰⁵ Ag	41.29d	c	5.33 ± 0.69
¹⁰⁰ Pd	87.12h	c	1.24 ± 0.27
¹⁰⁰ Rh	20.8h	c	3.97 ± 0.44
¹⁰⁰ Rh	20.8h	i	2.68 ± 0.28
^{99m} Rh	4.7h	c	2.41 ± 0.28
⁹⁷ Ru	69.6h	c	3.13 ± 0.28
⁹⁶ Tc	4.28d	i(m+g)	1.73 ± 0.20
^{93m} Mo	6.85h	i(m)	1.61 ± 0.13
⁹⁰ Nb	14.6h	c	2.58 ± 0.22
⁸⁹ Zr	78.41h	c	3.46 ± 0.28
⁸⁸ Zr	83.4d	c	2.56 ± 0.27
⁸⁸ Y	106.65d	c	3.49 ± 0.34
⁸⁸ Y	106.65d	i(m+g)	1.56 ± 0.22
⁸⁷ Y	79.8h	c	4.13 ± 0.34
⁸³ Sr	32.41h	c	1.96 ± 0.93
⁸⁴ Rb	32.77d	i(m+g)	1.31 ± 0.14
⁸³ Rb	86.2d	c	3.34 ± 0.58
^{82m} Rb	6.472h	i(m)	1.89 ± 0.17
⁷⁷ Kr	74.4m	c	1.71 ± 0.18
⁷⁵ Se	119.77d	c	2.38 ± 0.22
⁷³ Se	7.15h	c	1.03 ± 0.11
⁷⁴ As	17.77d	c	1.38 ± 0.16
^{69m} Zn	13.76h	i(m)	0.42 ± 0.038
⁵⁴ Mn	312.12d	i	2.51 ± 0.42
⁵¹ Cr	27.704d	c	4.5 ± 1.4

Continuation of Table 2

Product	T _{1/2}	Type	Yield (mb)
⁴⁸ V	15.973d	c	0.557 ± 0.062
⁴⁸ Sc	43.67h	i	0.668 ± 0.091
⁴³ K	22.3h	c	0.681 ± 0.084
²⁸ Mg	20.91h	c	0.91 ± 0.089
²⁴ Na	14.959h	c	4.09 ± 0.34
⁷ Be	53.29d	i	8.7 ± 1.0

Simulation of experimental results

Simulation techniques are of essential importance when forming the set of nuclear constants to be used in designing the ADS facilities, because they are universal and save much time and labour. At the same time, the present-day accuracy and reliability of the simulated results are inferior to experiment. Besides, the simulation codes are of different abilities to work when used to study the reactions that are of practical importance.

Considering the above, the present work is primarily aimed at verifying the simulation codes used most extensively for the above purpose with a view to not only estimating their ability to work when applied to the issues discussed here, but also opening up ways to improve them.

The following eight simulation codes were examined to meet these requirements:

- the CEM95 cascade-exciton code [7],
- the CASCADE cascade-evaporation-fission-transport code [8],
- the INUCL cascade-preequilibrium-evaporation-fission code [9],
- the LAHET (ISABEL and Bertini options) cascade-evaporation-fission code [10],
- the YIELDX semi-phenomenological code [11],
- the CASCADE/INPE cascade-preequilibrium-evaporation-fission-transport code [12],
- the CEM2k cascade-exciton code [16], a last modification of the CEM95 code,

Contrary to the simulation results, the experimental data include not only the independent, but also (and mainly) cumulative and the supra cumulative yields of residual product nuclei. To get a correct comparison between the experimental and simulation results, theoretical cumulative yields must be calculated on the basis of the simulated independent yields.

Since any branched isobaric chain can be presented to be a superposition of a few linear chains, the simulated cumulative and supra cumulative yields of a n-th nuclide can be calculated as

$$\sigma_n^{cum} = \sigma_n^{ind} + \sum_{i=1}^{n-1} \sigma_i^{ind} \prod_{j=i}^{n-1} \nu_j, \quad (7)$$

$$\sigma_n^{cum*} = \sigma_n^{ind} + \frac{\lambda_{n-1}}{\lambda_{n-1} - \lambda_n} \nu_{n-1} \times \left[\sigma_{n-1}^{ind} + \sum_{i=1}^{n-2} \left(\sigma_i^{ind} \prod_{j=i}^{n-2} \nu_j \right) \right]. \quad (8)$$

Table 3: The yields (mb) of some products in the 1 GeV proton-irradiated ^{208}Pb inferred from measurements at different laboratories; the ZSR and GSI data are taken from [6], the ITEP data are our present results

Product nuclide	ZSR Hannover	ITEP	GSI Darmstadt
^{200}Tl	22.3 ± 6.1	22.7 ± 1.5	$17.0 \pm 0.4(1.6)$
^{196}Au	3.88 ± 0.47	4.13 ± 0.35	$4.0 \pm 0.1(0.4)$
^{194}Au	6.85 ± 0.92	7.06 ± 0.75	$6.3 \pm 0.2(0.6)$
^{148}Eu	0.104 ± 0.04	–	$0.075 \pm 0.005(0.010)$
^{144}Pm	0.068 ± 0.013	–	$0.036 \pm 0.003(0.006)$

The branching ratios of the decay chains were retrieved from [13]. To get a correct comparison between results by different codes, the calculations were renormalized to unified cross sections for proton-nucleus inelastic interactions from [14].

If an experiment-simulation difference of not above 30% ($0.77 < \sigma_{calc}/\sigma_{exp} < 1.3$) is taken to be the coincidence criterion [15], the simulation accuracy can be presented to be the ratio of the number of such coincidences to the number of the comparison events. The 30% level meets the accuracy requirements of the cross sections for nuclide production to be used in designing the ADS plants, according to [15]. The mean simulated-to-experimental data ratio can be used as another coincidence criterion:

$$\langle F \rangle = 10^{\sqrt{\langle \log(\sigma_{cal,i}/\sigma_{exp,i})^2 \rangle}}, \quad (9)$$

with its standard deviation

$$S(\langle F \rangle) = \langle (\log(\sigma_{cal,i}/\sigma_{exp,i}) - \log(\langle F \rangle))^2 \rangle, \quad (10)$$

where $\langle \rangle$ designates averaging over all N_S number of the experimental and simulated results used in a comparison.

The mean ratio $\langle F \rangle$ together with its standard deviation $S(\langle F \rangle)$ defines the interval $[\langle F \rangle: S(\langle F \rangle), \langle F \rangle \times S(\langle F \rangle)]$ that covers about 2/3 of the simulation-to-experiment ratios.

The two criteria are considered sufficient to derive conclusions about the predictive power of a given code. The default options were committed to practical usage of the simulation codes.

Comparison of data with simulation results

The results obtained with the above-mentioned codes are presented in:

- Figs. 5 and 6, that show results of a detailed comparison between the simulated and experimental radioactive product yields;
- Figs. 7 and 8, that show the simulated mass distributions of reaction products together with the measured cumulative (and supra cumulative) yields of the products that are at an immediate proximity to the stable isobar of a given mass (the sum of such yields from either

Table 4: Comparison statistics for ^{208}Pb and ^{nat}W

Code	Pb, $E_p = 1.0$ GeV $N_T = 116, N_G = 95$			W, $E_p = 2.6$ GeV $N_T = 107, N_G = 93$		
	$N_{C_{1.3}}/N_{C_{2.0}}/$ $/N_S$	$\langle F \rangle$	$S(\langle F \rangle)$	$N_{C_{1.3}}/N_{C_{2.0}}/$ $/N_S$	$\langle F \rangle$	$S(\langle F \rangle)$
LAHET	41/65/90	2.06	1.78	13/51/90	2.52	1.83
CEM95	–	–	–	28/66/81	2.51	2.23
CEM2k	38/58/66	1.62	1.44	17/60/84	2.24	1.73
CASCADE	33/60/86	2.28	1.90	48/71/91	2.24	2.04
CASCADE/INPE	36/66/84	1.84	1.56	–	–	–
INUCL	29/54/90	2.87	2.16	38/58/86	3.78	3.23
YIELDX	30/54/90	2.87	2.24	25/60/93	2.04	1.58

sides in case both left- and right-hand branches of the chain are present). Obviously, the displayed simulation results do not contradict the experimental data if calculated values run above the experimental data and follow a general trend of the latter. This is because the direct γ -spectroscopy method used here identifies only radioactive products, that, as a rule, represents a significant fraction of the total mass yield, but, should a stable isobar of the given mass be produced, the γ -spectroscopy data are never equal to the total mass yield;

- In Fig. 9, that shows the experimental and simulated independent yields of reaction products in the form of isotopic mass distributions for several elements.

Table 4 presents the statistics of our comparison between the experimental and simulated reaction product yields in the thin ^{208}Pb and ^{nat}W samples irradiated by 1.0 GeV and 2.6 GeV protons, respectively. Namely, it shows the total number of measured yields, N_T ; the number of the measured yields selected to compare with calculations, N_G ; the number of the product nuclei whose yields were simulated by a particular code, N_S ; the number of the comparison events when the simulated data differ from the experimental results by not above 30%, $N_{C_{1.3}}$; the number of the comparison events when the simulated data differ from the experimental results by not more than a factor of 2.0, $N_{C_{2.0}}$.

Since about 30% of all measured secondary nuclei are not spallation reaction products, an important criterion of the codes is their ability to simulate the high-energy fission and fragmentation processes. Among the codes used here, LAHET, CASCADE, INUCL, CASCADE/INPE, and YIELDX simulate both spallation and fission. The CEM95 and CEM2k codes simulate spallation only, which is explicitly reflected in a smaller number of the products simulated (the parameter N_S in Table 4 and in the shapes of the simulation curves in Figs. 5-8).

The following conclusions follow from our analysis of the experiment-to-simulation comparison results presented in Table 4 and in Figs. 5-9:

1. Generally, all codes can quite adequately simulate the weak spallation reactions (the $A \geq 180$ products for ^{208}Pb and the $A \geq 150$ products for ^{nat}W), with the simulation results differing from experimental data within a factor of 2.

2. In the deep spallation region ($150 < A < 180$ for ^{208}Pb and $110 < A < 150$ for ^{nat}W), the simulation codes are of very different predictive powers, namely,
 - the LAHET (when not shown explicitly as “Bertini”, all results by LAHET are of the ISABEL option), CEM2k, CASCADE/INPE, and YIELDX predictions are actually the same as the experimental data;
 - the CASCADE code simulates the $A > 160$ product yields adequately. Below $A = 160$, however, the simulated data get underestimated progressively (up to a factor of 5) compared with experiment (see Fig. 7);
 - the INUCL code underestimates the yields of all the products by a factor of 2-10 in all the above mass ranges (see Figs. 7 and 8).
3. In the mass range characteristic of the fission products ($50 < A < 150$ for ^{208}Pb and $30 < A < 110$ for ^{nat}W), the INUCL code predictions are in the best agreement with experiment when describing the yields from ^{208}Pb . As a rule, the INUCL-simulated results differ from the data by not above a factor of 1.5. In the case of ^{nat}W , however, the prediction quality deteriorates substantially. The LAHET-simulated yields are underestimated by a factor of 1.5-10.0 for Pb (Figs. 5 and 7) in the whole fission product mass region and for $A < 60$ in the case of W (Figs. 6 and 8) but are overestimated several times for fission fragments with $A > 60$ from W. The YIELDX-simulated yields are either under- or over-estimated by a factor of up to 30 without showing any physical regularities. The CASCADE/INPE-simulated yields of the $130 < A < 150$ reaction products are strongly underestimated (up to 1-2 orders of magnitude), while the simulated $40 < A < 130$ product yields agree with the data within a factor of 2, as a rule. Generally, all the codes exhibit the feature noted above for INUCL, namely, the yield prediction quality in the case of ^{nat}W is much worse compared with ^{208}Pb , probably, because the fission cross sections of high-excited compound nuclei with very low fissility are difficult to calculate.
4. The last version of the improved cascade-exciton model code, CEM2k [16], shows the best agreement with the 1 GeV Pb-data in the spallation region, especially for the isotopic mass distributions (Fig. 9). At 2.6 GeV (W-target), it overestimates the expected experimental fission cross section of about 41 mb [17] by a factor of 6. This overestimation of the fission cross section causes an underestimation of the yield of nuclei which are most likely to fission (with a very low fissility) at the evaporation stage of a reaction, after the cascade and preequilibrium stages, i.e., for $147 < A < 175$ (see Fig. 6). Similar disagreement with the 2.6 GeV W-data one can see as well for LAHET and CEM95, that is also related with an overestimation of the fission cross section at 2.6 GeV (see Figs. 6 and 8). The code CEM2k is still under development, its problem with the overestimation of fission cross sections at energies above 1 GeV has yet to be solved, and it has to be complemented with a model of fission fragment production, to be able to describe as well fission products.

Conclusion

The trends shown by the advances in the nuclear transmutation of radioactive wastes and Spallation Neutron Source (SNS) facilities permit us to expect that the accumulation and analysis study of nuclear data for ADS facilities will have the same rise of academic interest and

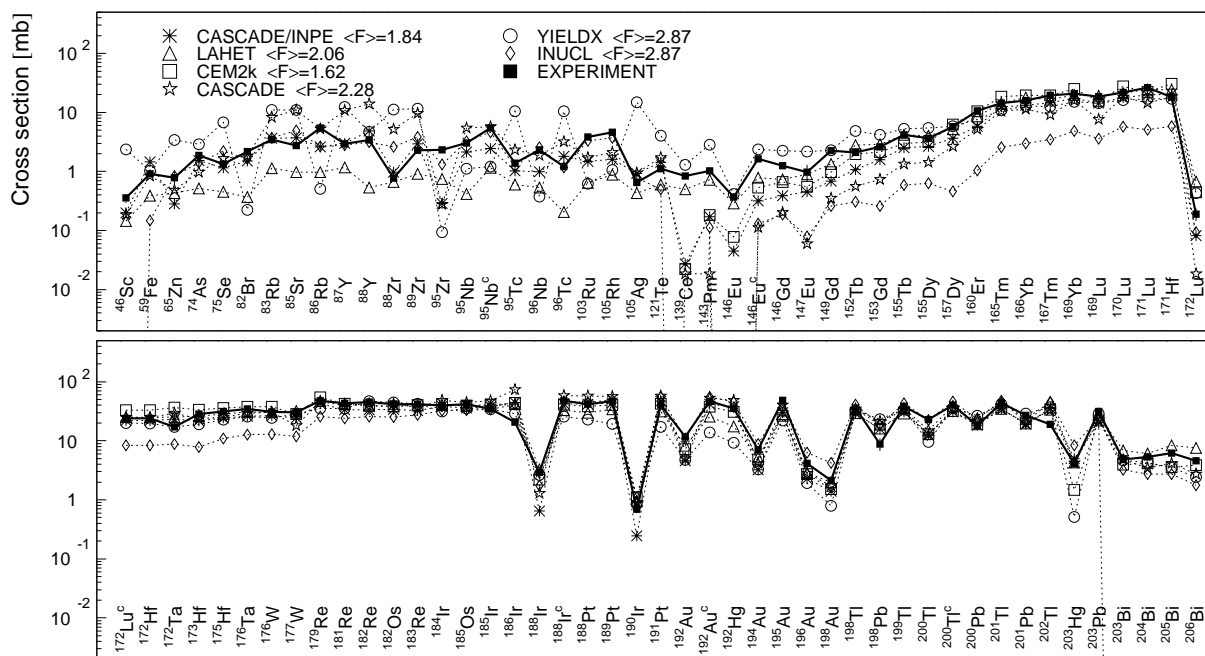


Figure 5: Product comparison between the experimental (closed symbols) and simulated (open symbols) yields of radioactive reaction products from ^{208}Pb irradiated with 1 GeV protons. The cumulative yields are labeled with a “c” when the respective independent yields are also shown.

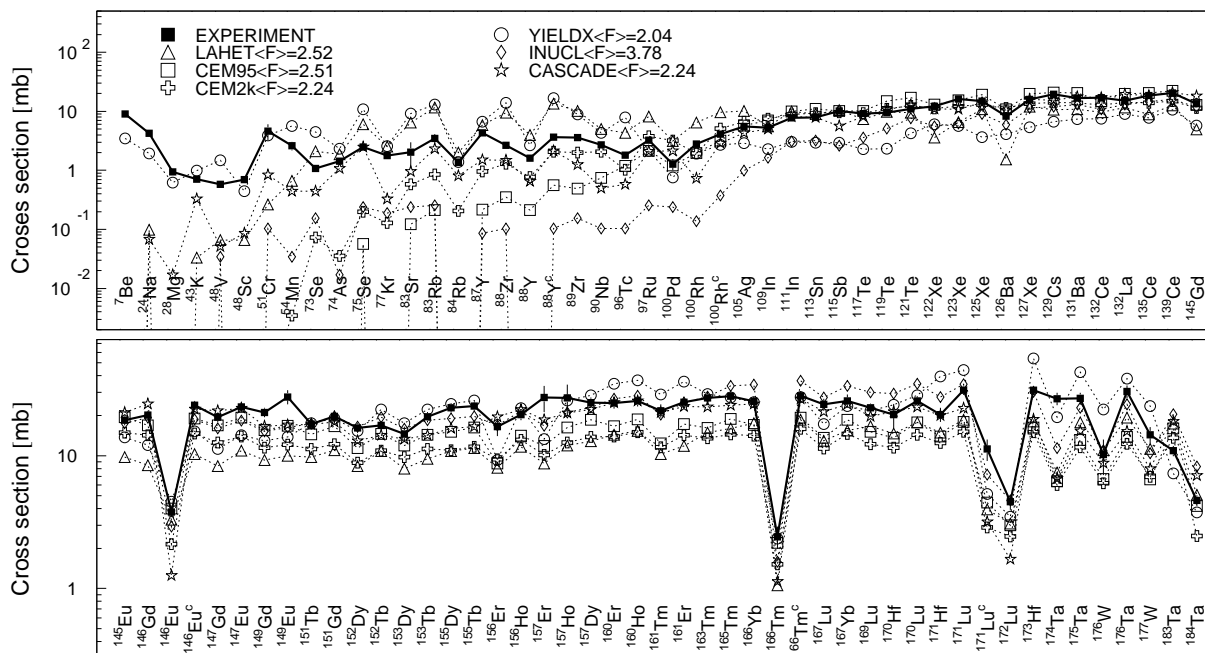


Figure 6: Product comparison between the experimental (closed symbols) and simulated (open symbols) yields of radioactive reaction products from ^{nat}W irradiated with 2.6 GeV protons. The cumulative yields are labeled with a “c” when the respective independent yields are also shown.

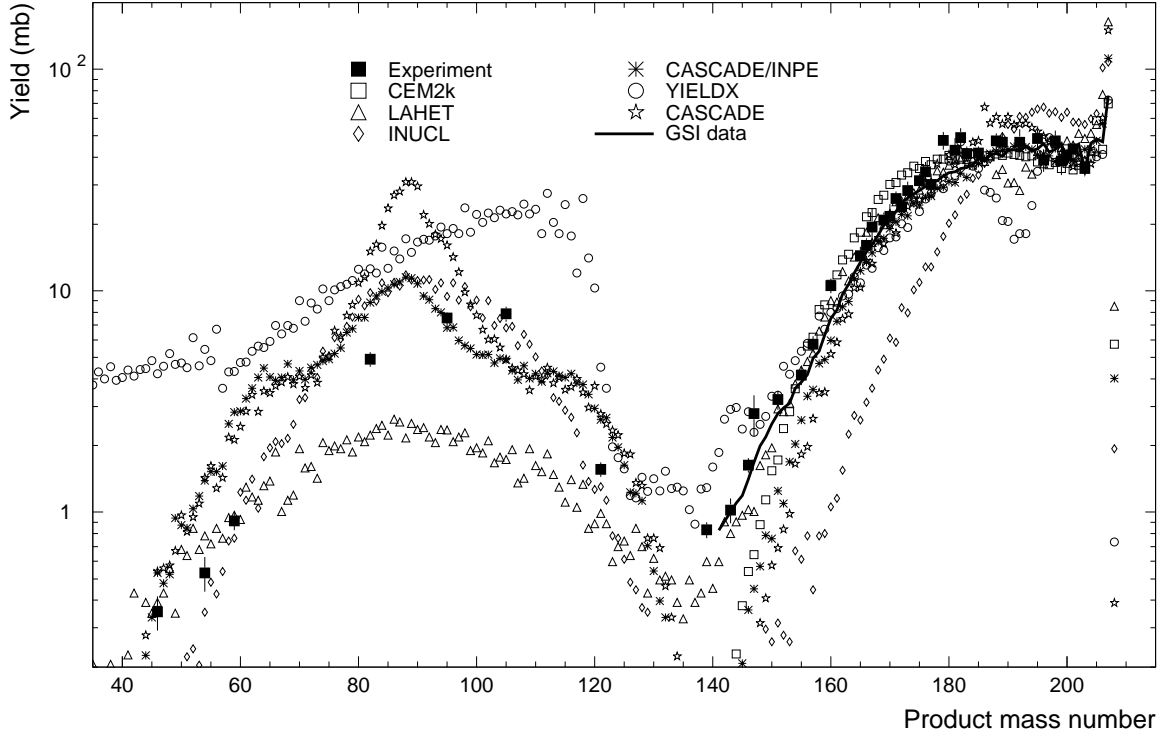


Figure 7: Measured and calculated by the codes mass product yields from ^{208}Pb irradiated with 1.0 GeV protons. For comparison, the GSI data from [6] are shown as well.

practical commitments as in the nuclear reactor data during the last five decades. Therefore, the experimental data on the yields of the proton-induced reaction products as applied to the ADS and SNS main targets and structure materials are urgent to accumulate. It should be emphasized that the charge distributions in the isobaric decay chains are important to study as well. The data thus obtained would make it possible, first, to raise the information content of the comparisons between the experimental and simulated results and, second, to lift the uncertainties in experimental determination of the cumulative yields by establishing unambiguous relations between σ^{cum} and σ^{cum*} for many of the reaction product masses.

Regarding the codes benchmarked here, one may conclude that none of them agree well with the data in the whole mass region of product nuclides and all should be improved further. The new CEM2k code developed recently at Los Alamos [16] agrees with our data in the spallation region the best of the codes tested. But CEM2k has yet to be completed by a model of fission fragmentation, to become applicable in the fission-product region as well.

Acknowledgement

The authors are grateful to Prof. Vladimir Artisyuk (Tokyo Institute of Technology) for consulting and discussion our results on simulation-to-experimental comparisons.

The work was carried out under the ISTC Project #839 supported by the European Community, Japan (JAERI), Norway and, partially, by the U. S. Department of Energy.

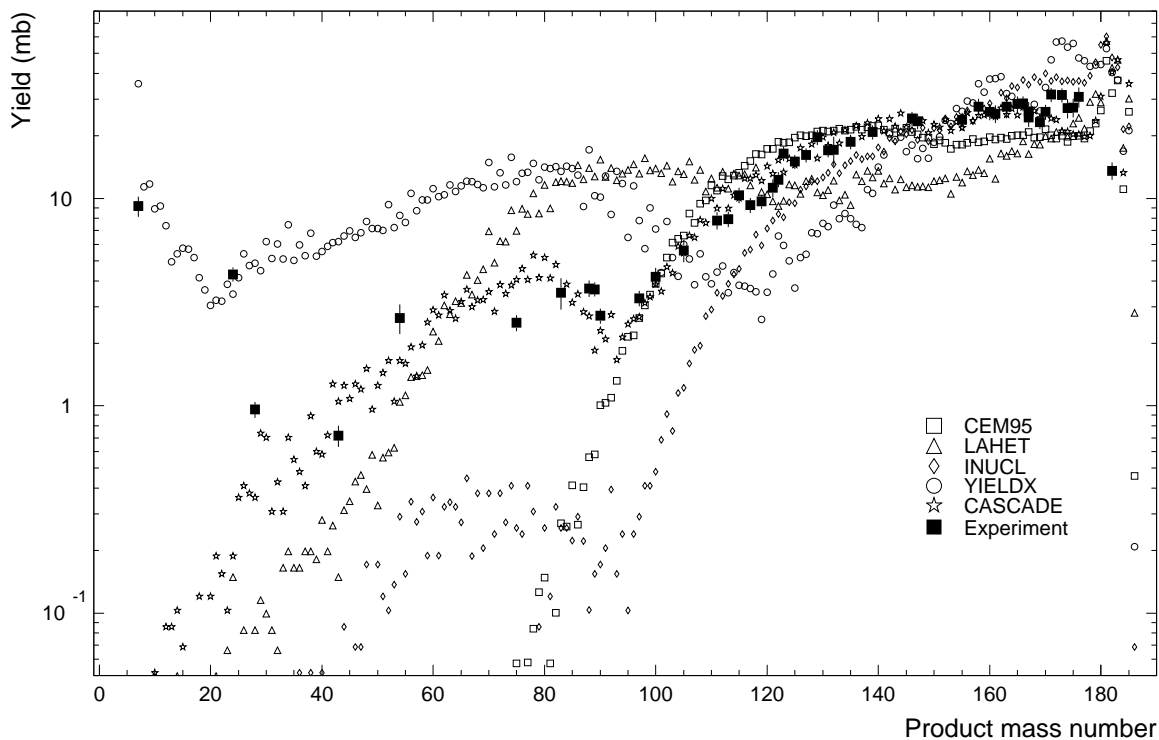


Figure 8: Measured and calculated via the codes mass product yields from ^{nat}W irradiated with 2.6 GeV protons.

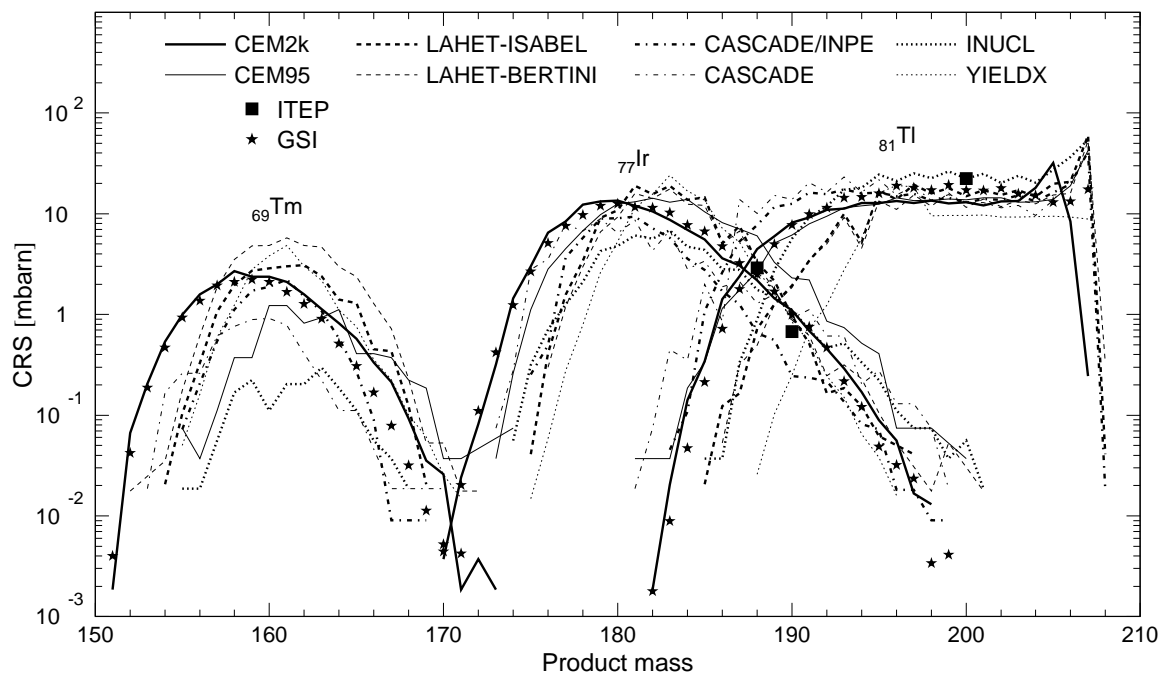
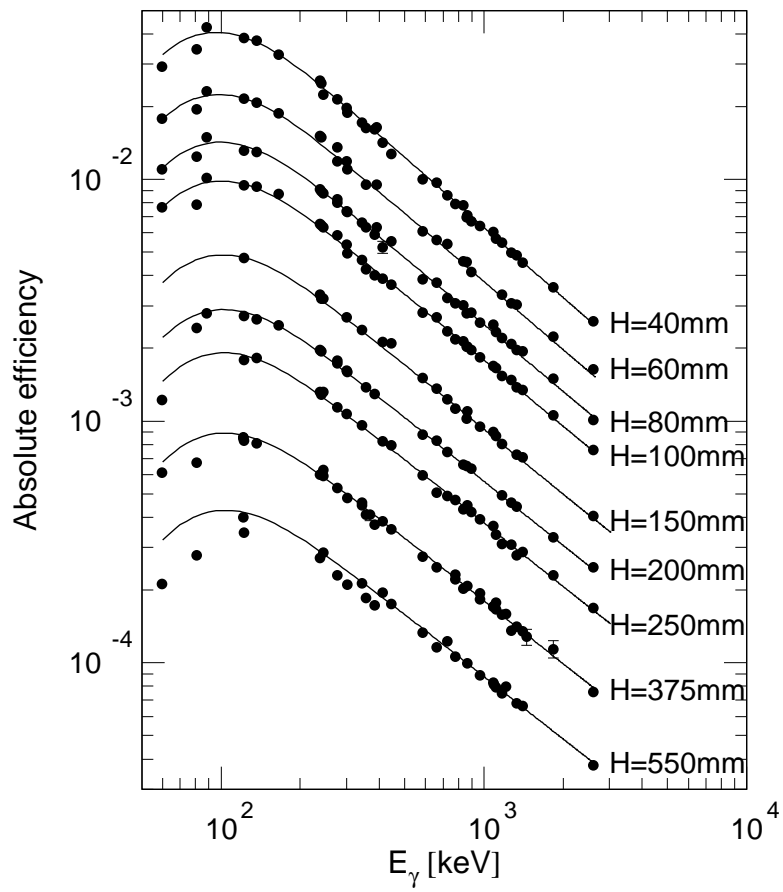


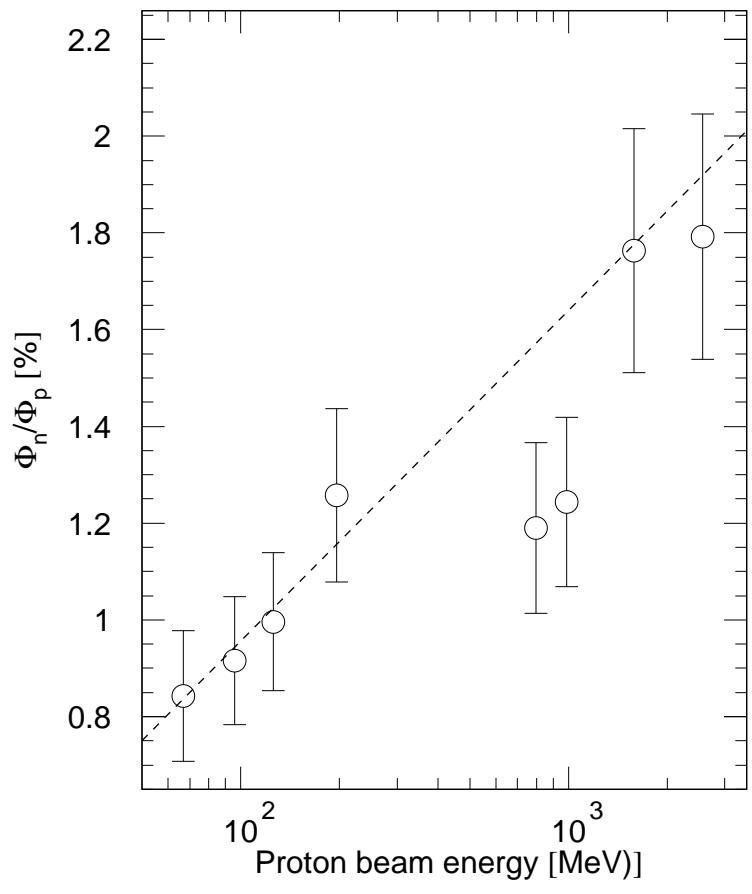
Figure 9: Isotopic mass distributions of the reaction products in ^{208}Pb . The rich, inverse-kinematics, GSI data from [6] are shown by filled stars.

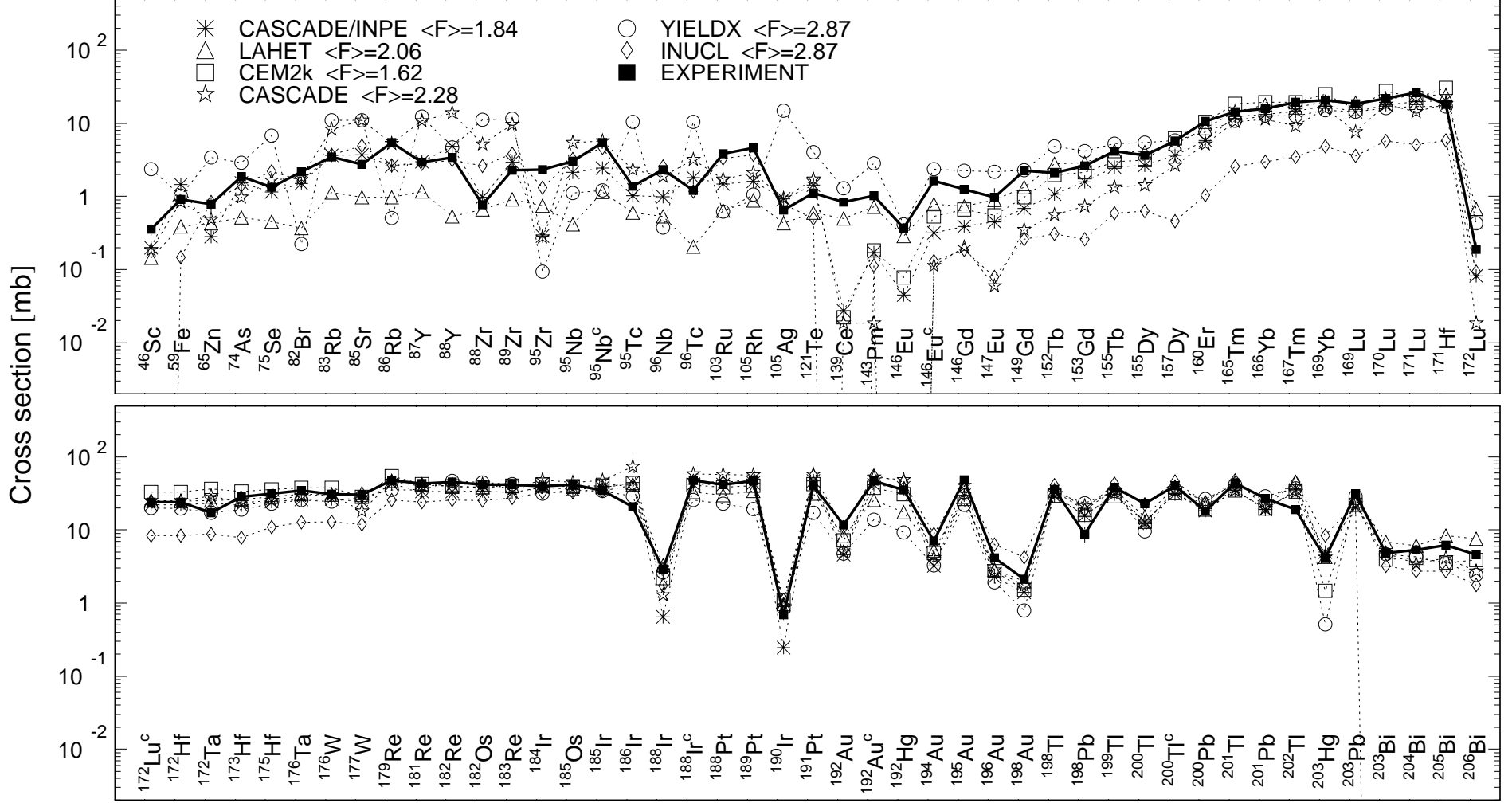
References

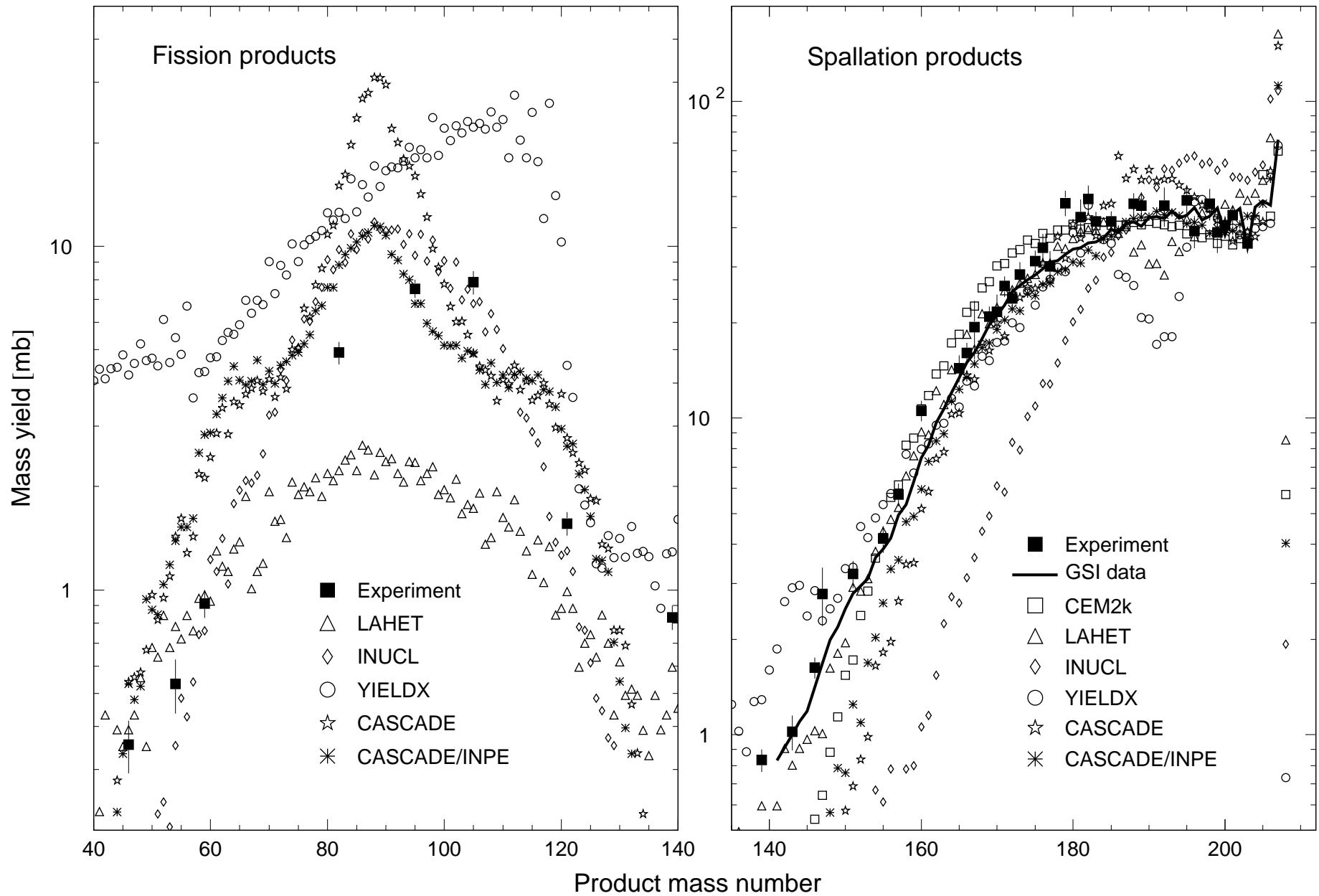
- [1] Gregory J. Van Tuyle, “ATW Technology Development & Demonstration Plan”, LANL Report LA-UR-99-1061, Los Alamos (1999); “ATW Technology & Scenarios”, LANL Report LA-UR 99-771, Los Alamos (1999).
- [2] T. Mukaiyama, “OMEGA Program in Japan and ADS Development at JAERI”, Proc. 3rd Int. Conf. on Accelerator-Driven Transmutation Technologies and Applications (ADTT’99), Praha, 7-11 June 1999, paper Mo-I-5.
- [3] M. Salvatores, “Strategies for the Back-End of the Fuel Cycle: A Scientific Point of view”, Proc. 3rd Int. Conf. on Accelerator-Driven Transmutation Technologies and Applications (ADTT’99), Praha, 7-11 June 1999, paper Mo-I-4.
- [4] Yu. E. Titarenko, O. V. Shvedov, M. M. Igumnov, S. G. Mashnik, E. I. Karpikhin, V. D. Kazaritsky, V. F. Batyaev, A. B. Koldobsky, V. M. Zhivun, A. N. Sosnin, R. E. Prael, M. B. Chadwick, T. A. Gabriel, and M. Blann, “Experimental and Computer Simulation Study of the Radionuclides Produced in Thin ^{209}Bi Targets by 130 MeV and 1.50 GeV Proton-Induced Reactions,” Nucl. Instr. Meth. A **414**, 73 (1998).
- [5] M. Gloris, R. Michel, U. Herpers, F. Sudbrok, and D. Filges, “Production of Residual Nuclei from Irradiation of Thin Pb-Targets with Protons up to 1.6 GeV”, Nucl. Instr. Meth. B **113**, 429 (1996); R. Michel, M. Gloris, H.-J. Lange, I. Leya, M. Lüpke, U. Herpers, B. Dittrich-Hannen, R. Rösel, Th. Schiekkel, D. Filges, P. Dragovitsch, M. Suter, H.-J. Hofmann, W. Wölfl, P. W. Kubik, H. Baur, and R. Wieler, “Nuclide Production by Proton-Induced Reactions on Elements ($6 \leq Z \leq 29$) in the Energy Range from 800 to 2600 MeV”, Nucl. Instr. Meth. B **103**, 183 (1995).
- [6] W. Wlazole, T. Enqvist, P. Armbruster, P. Armbruster, J. Benlliure, M. Bernas, A. Boudard, S. Czajkowski, R. Legrain, S. Leray, B. Mustapha, M. Pravikoff, F. Rejmund, K.-H. Schmidt, C. Stéphan, J. Taieb, L. Tassan-Got, and C. Volant, “Cross Sections of Spallation Residues Produced in 1A GeV ^{208}Pb on Proton Reactions,” Phys. Rev. Lett. **84**, 5736 (2000).
- [7] K. K. Gudima, S. G. Mashnik, and V. D. Toneev, “Cascade-Exciton Model of Nuclear Reactions,” Nucl. Phys. A **401**, 329 (1983); S. G. Mashnik, “User Manual for the Code CEM95”, JINR, Dubna, 1995; OECD Nuclear Energy Agency Data Bank, Paris, France (1995), <http://www.nea.fr/abs/html/iaea1247.html>; RSIC-PSR-357, Oak Ridge, TN (1995).
- [8] V. S. Barashenkov, Le Van Ngok, L. G. Levchuk, Zh. Zh. Musul’manbekov, A. N. Sosnin, V. D. Toneev, and S. Yu. Shmakov, “Cascade Program Complex for Monte-Carlo Simulation of Nuclear Processes Initiated by High Energy Particles and Nuclei in Gaseous and Condensed Matter,” JINR Report R2-85-173, Dubna (1985); V. S. Barashenkov, F. G. Zheregi, and Zh. Zh. Musul’manbekov, “The Cascade Mechanism of Interactions of High-Energy Nuclei,” Yad. Fiz. **39** (1984) 1133; V.S. Barashenkov, B.F. Kostenko and A.M. Zadorogny, “Time-Dependent Intranuclear Cascade Model,” Nucl. Phys. A **338**, 413 (1980).
- [9] G. A. Lobov, N. V. Stepanov, A. A. Sibirtsev, and Yu. V. Trebukhovskii, “Statistical Simulation of Interaction of Hadrons and Light Nuclei with Nuclei. Intranuclear Cascade Model,” Preprint ITEP-91, Moscow (1983); A. A. Sibirtsev, N. V. Stepanov, and Yu. V. Trebukhovskii, “Interaction of Particles with Nuclei. Evaporation Model,” Preprint ITEP-129,

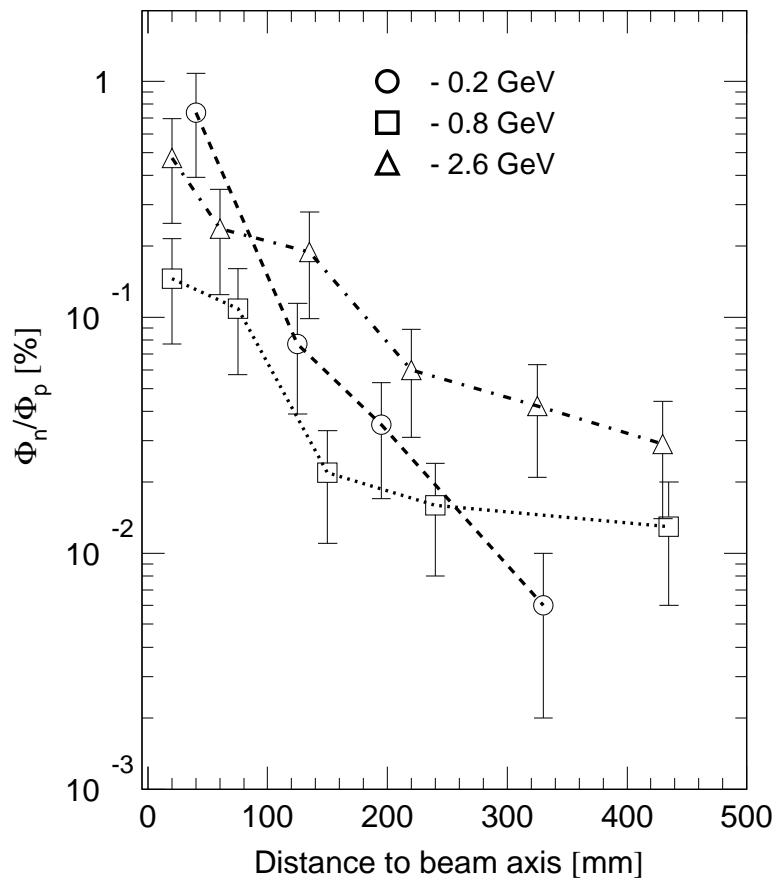
- Moscow (1985); N. V. Stepanov, “Statistical Simulation of High-Excited Nuclei Fission. I. Model Formulation,” Preprint ITEP-81, Moscow (1987); N. V. Stepanov, “Statistical Simulation of High-Excited Nuclei Fission. II. Calculation and Comparison with Experiment,” (in Russian) Preprint ITEP-55-88, Moscow (1988).
- [10] R. E. Prael and H. Lichtenstein, “User guide to LCS: The LAHET Code System,” LANL Report LA-UR-89-3014, Los Alamos (1989); see also the Web page at: <http://www-xdiv.lanl.gov/XTM/lcs/lahet-doc.html>.
- [11] C. H. Tsao, Private communication; R. Silberberg, C. H. Tsao, and A. F. Barghouty, “Updated Partial Cross Sections of Proton-Nucleus Reactions,” *Astrophys. J.*, **501**, 911 (1998); R. Silberberg and C. H. Tsao, “Partial Cross-Sections in High-Energy Nuclear Reactions, and Astrophysical Applications. I. Targets With $Z \leq 28$,” *Astrophys. J. Suppl.*, No. 220, **25**, 315 (1973); “Partial Cross-Sections in High-Energy Nuclear Reactions, and Astrophysical Applications. II. Targets Heavier Than Nickel,” *ibid*, p. 335.
- [12] V. S. Barashenkov, A. Yu. Konobeev, Yu. A. Korovin, and V. N. Sosnin, “CASCADE/INPE Code System,” *Atomnaya Énergiya* **87**, 283 (1999).
- [13] N. G. Gusev and P. P. Dmitriev, *Radioactive Chains: Handbook*, Energoatomizdat, Moscow, 1988.
- [14] J. R. Letaw, R. Silberberg, and C. H. Tsao, “Proton-Nucleus Total Inelastic Cross Sections: An Empirical Formula for $E > 10$ MeV,” *Astrophys. J. Suppl.*, **51**, 271 (1983).
- [15] A. Koning, “Nuclear Data Evaluation for Accelerator-Driven Systems”, Proc. 2d Int. Conf. on Accelerator-Driven Transmutation Technologies and Applications, 3-7 June 1996, Kalmar, Sweden, pp. 438-447.
- [16] The code CEM2k is briefly surveyed in S. G. Mashnik, L. S. Waters, and T. A. Gabriel, “Models and Codes for Intermediate Energy Nuclear Reactions,” Proc. 5th Int. Workshop on Simulating Accelerator Radiation Environments (SARE5), July 17–18, 2000, OECD Headquarters, Paris, France, and will be described by S. G. Mashnik and A. J. Sierk in a future paper.
- [17] A. V. Prokofiev, “Compilation and Systematics of Proton-Induced Fission Cross Section Data,” *Nucl. Instr. Meth. A*, submitted in December 1998, to be published in September 2000.



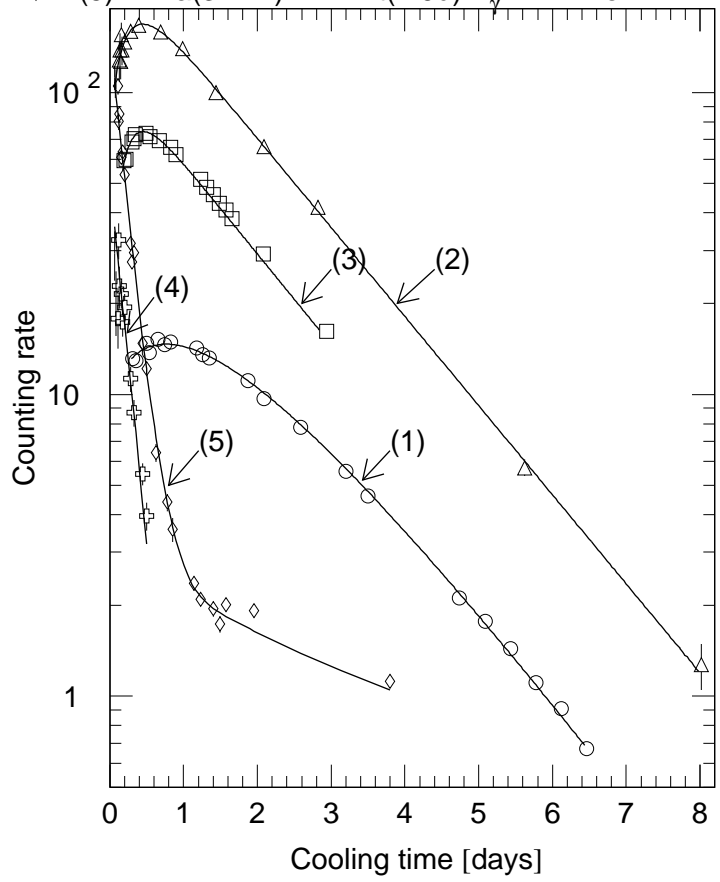


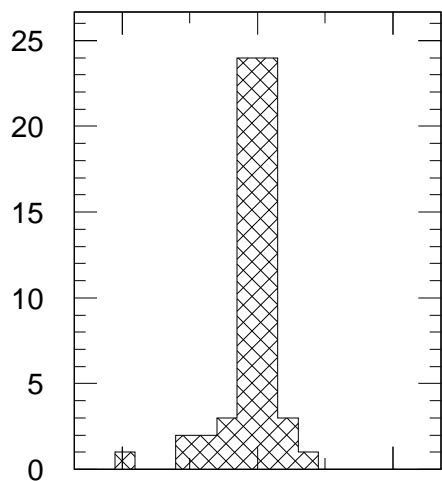




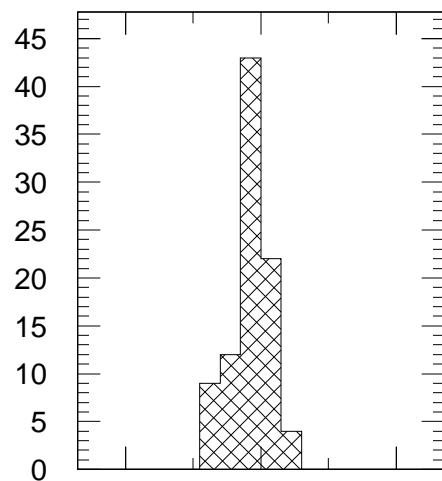


- (1) $^{192}\text{Hg}(4.85\text{h}) \rightarrow ^{192}\text{Au}(4.94\text{h}) E_{\gamma}=316.5\text{keV} \times 0.1 \times 4$
- △ (2) $^{188}\text{Pt}(10.2\text{d}) \rightarrow ^{188}\text{Ir}(41\text{h}) E_{\gamma}=2214.6\text{keV} \times 100 \times 0.1$
- (3) $^{173}\text{Ta}(3.14\text{h}) \rightarrow ^{173}\text{Hf}(23.6\text{h}) E_{\gamma}=123.7\text{keV}$
- ⊕ (4) $^{173}\text{Ta}(3.14\text{h}) E_{\gamma}=160.4\text{keV}$
- ◇ (5) $^{173}\text{Ta}(3.14\text{h}) + ^{191}\text{Pt}(2.9\text{d}) E_{\gamma}=172.2\text{keV}$

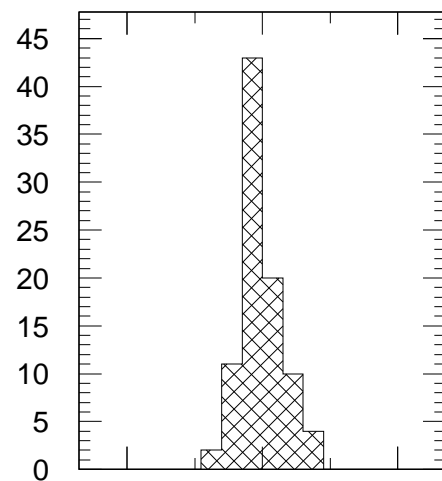




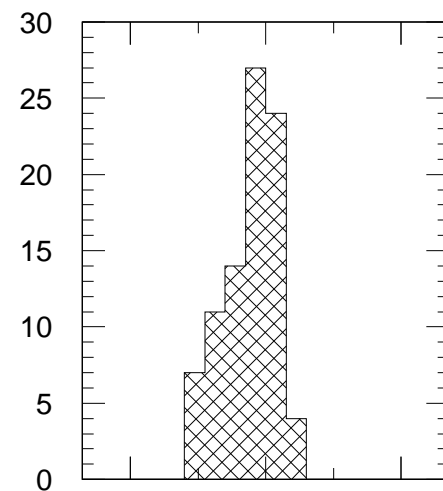
CEM95



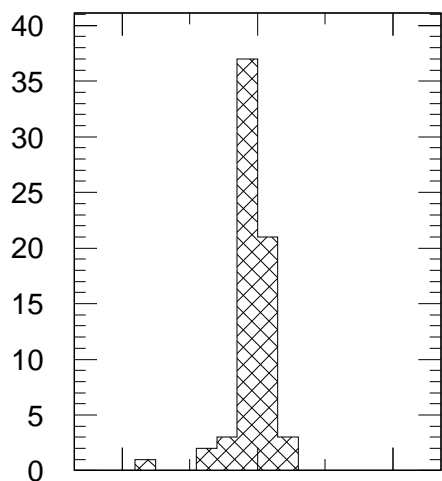
LAHET(ISABEL)



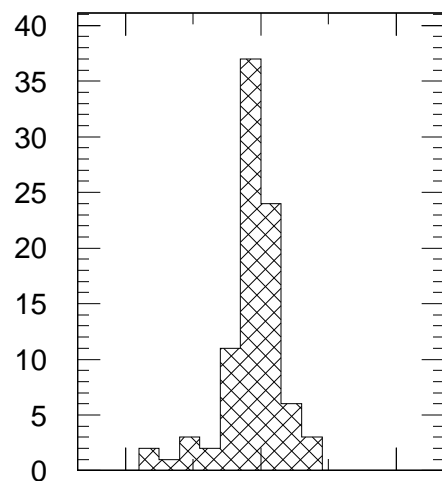
LAHET(BERTINI)



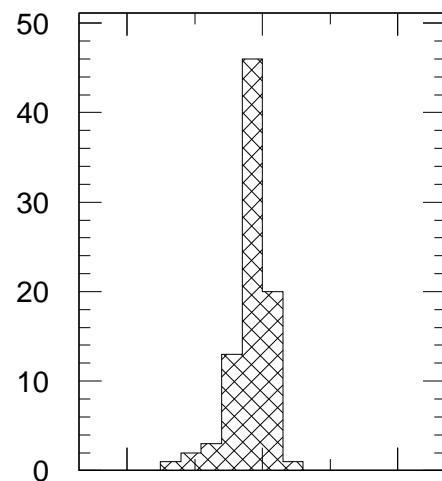
INUCL



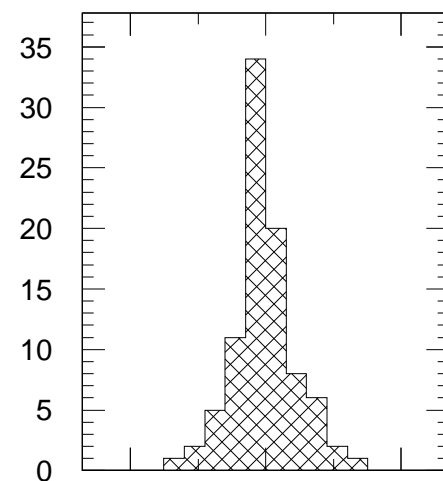
CEM2k



CASCADE



CASCADE/INPE



YIELDX

$\sigma_{\text{calc},i} / \sigma_{\text{exp},i}$

